Holographic light-quark energy loss in a spinning plasma

Yan-Qing Zhao (赵彦清)[1†] Zhou-Run Zhu (朱洲润)[2‡]

[1]College of Physics and Electronic Engineering, Hainan Normal University, Haikou 571158, China
[2]School of Physics and Telecommunications Engineering, Zhoukou Normal University, Zhoukou 466001, China

Abstract: In this work, we investigate light-quark energy loss in a strongly coupled plasma described by a spinning black-brane background obtained from the large-black-hole limit of the Myers-Perry geometry. The parameter a characterizes the boost or rotation of the dual fluid in this holographic setup and is related to the angular velocity in the corresponding limit. We employ two complementary probes, the falling-string and shooting-string descriptions, to compute the stopping distance and instantaneous energy loss of a light quark moving in directions either transverse or parallel to the local tangential-flow direction. The results show that light quarks lose energy more readily in a hot environment. For parallel propagation, a counter-propagating configuration enhances energy loss, whereas a co-propagating configuration suppresses it. For transverse propagation, increasing the magnitude of the rotational motion promotes energy loss. In addition, the instantaneous energy loss increases along the trajectory of the endpoint. These results describe classical probe dynamics in the local planar limit and do not include intrinsic-spin effects.

Keywords: AdS/CFT correspondence, light quark, spinning

DOI: **CSTR:**

CPC Accepted

I. INTRODUCTION

Heavy-ion collision experiments have provided strong evidence that a quark-gluon plasma (QGP) forms under extreme conditions [1−4]. One of the most informative probes of the QGP is jet quenching: energetic partons produced in the early stages of the collision lose energy while propagating through the hot, dense medium, resulting in the suppression of high-transverse-momentum hadrons [5−8]. Experimental data further indicate that the produced QGP behaves as a strongly coupled, nearly perfect fluid with a small ratio of shear viscosity to entropy density [9, 10]. This strongly coupled nature renders perturbative methods insufficient in certain regimes and motivates the use of nonperturbative approaches.

The AdS/CFT correspondence [11−13] provides a useful theoretical framework for studying strongly coupled plasma dynamics. In this framework, a finite-temperature, strongly coupled plasma is described holographically by a black hole geometry in asymptotically anti-de Sitter spacetime. Holographic methods have been extensively used to investigate parton energy loss and jet quenching in strongly coupled media [14, 15]. Several complementary observables and descriptions have been developed, including the jet quenching parameter [16, 17], the falling-string picture [18−21], and the shooting-string picture [22, 23]. The falling-string and shooting-string approaches are particularly useful for describing the energy loss and stopping distance of light quarks in a strongly coupled plasma [24−28].

In non-central heavy-ion collisions, the produced medium can carry a large orbital angular momentum, part of which may be transferred to the QGP, giving rise to a rotating, vortical system [29−33]. This has motivated increasing interest in the effects of rotation on deconfinement, heavy-quark dynamics, and parton energy loss [34−38]. In holography, rotating black hole backgrounds provide a natural setting for modeling such effects [39−43]. Previous studies have examined the thermodynamics of heavy quarks in spinning black hole backgrounds [44−46], and the jet-quenching parameter in such backgrounds has also been investigated [47]. However, most existing studies have focused either on heavy-quark observables or on the jet-quenching parameter. A systematic analysis of light-quark energy loss using both the falling-string and shooting-string approaches in a rotating background has not yet been carried out.

Received 2 September 2026; Accepted 4 November 2026

† E-mail: zhaoyanqing@hainnu.edu.cn
‡ E-mail: zhuzhourun@zknu.edu.cn

Content from this work may be used under the terms of the Creative Commons Attribution 3.0 licence. Any further distribution of this work must maintain attribution to the author(s) and the title of the work, journal citation and DOI. Article funded by SCOAP[3] and published under licence by Chinese Physical Society and the Institute of High Energy Physics of the Chinese Academy of Sciences and the Institute of Modern Physics of the Chinese Academy of Sciences and IOP Publishing Ltd

In this work, we study the holographic energy loss of a light quark in the local planar limit of the spinning Myers–Perry geometry, where the global rotational motion is represented by a local tangential plasma flow. The Myers-Perry black hole has a compact boundary with topology $S^3\times\mathbb{R}$ [42] and is dual to a gauge theory defined on this curved background. In the large black hole limit, the geometry locally reduces to a boosted Schwarzschild black brane, where the boost parameter is related to the rotation of the dual fluid. In this planar limit, the background is homogeneous and retains only the local tangential flow of the rotating plasma. The global rotation axis and the dependence on the distance from that axis are not retained. Consequently, spatial velocity gradients, fluid vorticity, centrifugal acceleration, and possible position-dependent temperature effects are beyond the scope of the present approximation. These effects would require the full Myers-Perry geometry or another nonuniform rotating background. Although the connection to QCD is not literal, this construction provides a holographic model for exploring how rotation affects the dynamics of a strongly coupled plasma. By working in a local patch of the boundary fluid, one can isolate the kinematic effect of the local tangential flow inherited from the global rotation and study the corresponding modification of light-quark energy loss. We analyze this problem using both the falling-string and shooting-string methods. In particular, we examine how the rotation parameter affects the light-quark stopping distance and energy loss rate. This comparison allows us to clarify the role of rotation in light-quark energy loss from two complementary holographic perspectives.

Throughout this work, the term light quark is used in the conventional sense of holographic energy-loss models employing classical probes. The calculation does not resolve the intrinsic spin of the probe and does not include spin–rotation or spin–vorticity couplings. The results describe stopping and energy dissipation within this approximation and do not constitute a complete description of spin-dependent light-quark dynamics in a vortical plasma.

The paper is organized as follows. In Sec. II, we review the Myers-Perry black hole background. In Sec. III, we study light-quark energy loss in the spinning background using the falling-string and shooting-string approaches. In Sec. IV, we present the conclusions and discussion.

II. SPINNING MYERS–PERRY BLACK HOLE BACKGROUND

We begin by briefly reviewing the rotating black-hole background considered by Hawking et al. [39], whose metric is given by

$$\begin{aligned} ds^2 =& -\frac{\Delta}{\rho^2}\left(dt_H-\frac{a\sin^2\theta_H}{\Xi_a}d\phi_H-\frac{b\cos^2\theta_H}{\Xi_b}d\psi_H\right)^2+\frac{\Delta_{\theta_H}\sin^2\theta_H}{\rho^2}\left(adt_H-\frac{r_H^2+a^2}{\Xi_a}d\phi_H\right)^2\\ &+\frac{\Delta_{\theta_H}\cos^2\theta_H}{\rho^2}\left(bdt_H-\frac{r_H^2+b^2}{\Xi_b}d\psi_H\right)^2+\frac{\rho^2}{\Delta}dr_H^2+\frac{\rho^2}{\Delta_{\theta_H}}d\theta_H^2\\ &+\frac{1+\frac{r_H^2}{R^2}}{r_H^2\rho^2}\left(abdt_H-\frac{b\left(r_H^2+a^2\right)\sin^2\theta_H}{\Xi_a}d\phi_H-\frac{a\left(r_H^2+b^2\right)\cos^2\theta_H}{\Xi_b}d\psi_H\right)^2, \end{aligned} \tag{1}$$

with

$$\begin{aligned} \Delta &= \frac{1}{r_H^2}(r_H^2+a^2)(r_H^2+b^2)\left(1+\frac{r_H^2}{R^2}\right)-2M,\\ \Delta_{\theta_H} &= 1-\frac{a^2}{R^2}\cos^2\theta_H-\frac{b^2}{R^2}\sin^2\theta_H,\\ \rho^2 &= r_H^2+a^2\cos^2\theta_H+b^2\sin^2\theta_H,\\ \Xi_a &= 1-\frac{a^2}{R^2},\Xi_b=1-\frac{b^2}{R^2}, \end{aligned} \tag{2}$$

where ϕ_H, ψ_H, and θ_H are the Hopf angular coordinates, and t_H, R, and r_H denote the time coordinate, the AdS radius, and the radial coordinate, respectively. The parameters a and b are rotation parameters associated with the two independent angular momenta. We consider the equal-angular-momenta case, $a=b$, which corresponds to the rotating Myers–Perry black hole [40, 41].

The calculations can be simplified by using the following coordinate system [48].

$$\begin{aligned} &t=t_H,\quad r^2=\frac{a^2+r_H^2}{1-\frac{a^2}{R^2}},\quad \theta=2\theta_H,\quad \phi=\phi_H-\psi_H,\\ &\psi=-\frac{2at_H}{R^2}+\phi_H+\psi_H,\quad b=a,\quad \mu=\frac{M}{(R^2-a^2)^3}. \end{aligned} \tag{3}$$

Equation (1) can be rewritten as follows:

CPC Accepted

$$ds^2 = -\left(1+\frac{r^2}{R^2}\right)dt^2 + \frac{dr^2}{G(\mathrm{r})} + \frac{r^2}{4}\left((\sigma^1)^2+(\sigma^2)^2+(\sigma^3)^2\right) + \frac{2\mu}{r^2}\left(dt+\frac{a}{2}\sigma^3\right)^2, \tag{4}$$

with

$$\begin{aligned} G(r) &= 1+\frac{r^2}{R^2} - \frac{2\mu\left(1-\frac{a^2}{R^2}\right)}{r^2} + \frac{2\mu a^2}{r^4}, \\ \mu &= \frac{r_h^4(R^2+r_h^2)}{2R^2r_h^2 - 2a^2(R^2+r_h^2)}, \\ \sigma^1 &= -\sin\psi d\theta + \cos\psi\sin\theta d\phi, \\ \sigma^2 &= \cos\psi d\theta + \sin\psi\sin\theta d\phi, \\ \sigma^3 &= d\psi + \cos\theta d\phi, \end{aligned} \tag{5}$$

where

$$-\infty < t < \infty,\ r_h < r < \infty,\ 0 \le \theta < \pi,\ 0 \le \phi < 2\pi,\ 0 \le \psi < 4\pi. \tag{6}$$

To take the planar limit, we introduce local coordinates

$$\begin{aligned} &t = \tau, \quad \frac{R}{2}(\phi-\pi) = x_1, \quad \frac{R}{2}\tan\left(\theta-\frac{\pi}{2}\right) = x_2, \\ &\frac{R}{2}(\psi-2\pi) = x_3, \quad r = \tilde{r}, \end{aligned} \tag{7}$$

where $(\tau, \tilde{r}, x_1, x_2, x_3)$ denote the new coordinates, which can be rescaled by β in the limit $\beta \to \infty$.

$$\begin{aligned} &\tau \to \beta^{-1}\tau, \quad x_1 \to \beta^{-1}x_1, \quad x_2 \to \beta^{-1}x_2, \\ &x_3 \to \beta^{-1}x_3, \quad \tilde{r} \to \beta\tilde{r}, \quad \tilde{r}_h \to \beta\tilde{r}_h. \end{aligned} \tag{8}$$

This coordinate transformation yields the planar black brane solution [42].

$$ds^2 = \frac{r^2}{R^2}\left(-d\tau^2 + dx_1^2 + dx_2^2 + dx_3^2 + \frac{r_h^4}{r^4\left(1-\frac{a^2}{R^2}\right)}\left(d\tau + \frac{a}{R}dx_3\right)^2\right) + \frac{R^2r^2}{r^4-r_h^4}dr^2, \tag{9}$$

where a is the boost parameter and r_h denotes the horizon radius. Setting $a=0$ recovers the Schwarzschild black brane.

To express Eq. (9) in dimensionless form, we introduce the dimensionless coordinates $\tilde{\tau} = \frac{\tau}{R}, \tilde{x}_i = \frac{x_i}{R}$, $\tilde{z} = \frac{R}{r}$ and the dimensionless rotation parameter $\tilde{a} = \frac{a}{R}$. We also rescale the line element as $d\tilde{s}^2 = \frac{ds^2}{R^2}$. For notational simplicity, the tildes are omitted in what follows,

$$ds^2 = \frac{1}{z^2}\left(-d\tau^2 + dx_1^2 + dx_2^2 + dx_3^2 + \frac{z^4}{z_h^4(1-a^2)}(d\tau + a dx_3)^2\right) + \frac{z_h^4}{z^2(z_h^4-z^4)}dz^2. \tag{10}$$

The metric in Eq. (10) represents the local planar limit of the globally rotating Myers–Perry geometry. In this limit, the original angular motion is described as a local tangential plasma flow, with x_3 denoting the local flow direction. The dimensionless parameter $a = \Omega R$ [42] characterizes the local boost, or flow velocity. This approximation captures the local relative motion between the probe and the rotating plasma, whereas effects associated with finite distance from the rotation axis, spatial velocity gradients, vorticity, centrifugal acceleration, and finite-size geometry lie beyond the strict planar limit. All variables below are dimensionless quantities obtained by scaling with R, and the rescaled symbols are written without tildes.

The corresponding dimensionless Hawking temperature is

$$T = \frac{\sqrt{1-a^2}}{z_h\pi}, \tag{11}$$

III. LIGHT QUARK ENERGY LOSS IN THE SPINNING BLACK HOLE BACKGROUND

The purpose of this section is to investigate how the relative motion between an energetic light quark and the local plasma flow affects the quark stopping distance and instantaneous energy-loss rate. We consider propagation both transverse and parallel to the local flow direction and employ two complementary holographic descriptions: the falling-string approach for the stopping distance and the shooting-string approach for the instantaneous energy-loss rate. The calculation performed below is not a passive coordinate transformation of a single

CPC Accepted

jet–medium configuration. For each value of a, we use the same boundary laboratory coordinates (τ, x_1, x_2, x_3) and, in the falling-string calculation, keep the laboratory-frame jet energy, momentum magnitude, and propagation direction fixed. In the ultrarelativistic limit, the transverse and parallel jet momenta are chosen as

$$q_\perp^\mu = (\omega, |\vec{q}|, 0, 0), \qquad q_\parallel^\mu = (\omega, 0, 0, |\vec{q}|), \qquad \omega = |\vec{q}|. \tag{12}$$

Throughout this work, the energetic probe is modeled as a classical string configuration. The calculation describes the stopping and energy dissipation of an energetic quark excitation but does not introduce an explicit intrinsic spin degree of freedom. Consequently, spin–rotation and spin–vorticity couplings are not included. The dependence on a should therefore be interpreted as the interaction of the probe with the local tangential flow, rather than as a calculation of spin-dependent dynamics in a vortical plasma.

A. Falling string

In this subsection, we apply the method developed in [19, 20] to study light-quark jet quenching in a spinning black-hole background. The key idea is to examine the stopping distance of the image jet induced by a massless source field. In the WKB approximation, this corresponds to a massless particle following a null geodesic. As the wave packet of the gauge field falls into the horizon, the corresponding boundary jet dissipates and eventually loses its energy. Thus, the stopping distance is defined as the maximum distance that the jet can travel before stopping.

In the WKB approximation, we assume that the wave packet of the massless gauge field in the gravity dual is well localized in momentum space. This assumption allows the wave function to be factorized as

$$A_j(\tau, z) = \exp\left[\frac{i}{\hbar}\left(q_k x_k + \int dz q_z\right)\right] \tilde{A}_j(\tau, z), \tag{13}$$

where q_k denotes the four-momentum, which is conserved owing to the translational invariance of the metric in the four boundary dimensions. q_z is the momentum component in the holographic direction. $\tilde{A}_j(\tau, z)$ is a slowly varying function of τ and z, and the indices j,k label the four spacetime coordinates.

The metric in Eq. (10) describes the local tangential-flow sector of the globally rotating plasma, with x_3 chosen along the local flow direction. We therefore investigate the energy loss of light quarks in two configurations. In the transverse case, the light quark propagates along x_1 or x_2. In the parallel case, it propagates along the local flow direction x_3.

We first consider the transverse case. In the classical limit $\hbar \to 0$, the wave packet follows a null geodesic.

$$0 = ds^2 = g_{ij} dx^i dx^j + g_{zz} dz^2, \tag{14}$$

yielding

$$\frac{dz}{d\zeta} = \frac{1}{\sqrt{g_{zz}}}\left[-g_{ij}\frac{dx^i}{d\zeta}\frac{dx^j}{d\zeta}\right]^{1/2}, \tag{15}$$

where ζ is an affine parameter along the trajectory, $g_{zz} = \dfrac{1}{z^2 D(z)}$, and $D(z) = 1 - \dfrac{z^4}{z_h^4}$. Because the metric is invariant under four-dimensional translations, the corresponding four-momentum components are conserved. Thus, $g_{ij}\dfrac{dx^j}{d\zeta}$ is conserved and proportional to q_i, which leads to

$$\frac{dx^i}{d\zeta} \propto g^{ij} q_j. \tag{16}$$

Dividing (16) by (15) yields

$$\frac{dx^i}{dz} = \sqrt{g_{zz}}\frac{g^{ij} q_j}{\left(-q_k g^{kl} q_l\right)^{1/2}}. \tag{17}$$

We next compute the stopping distance. Substituting the metric (10) into (17) yields the stopping distance for the transverse case in the spinning black hole background,

$$x_\perp = \int_0^{z_h} dz \frac{|\vec{q}|}{\sqrt{(1 + a^2 F(z))\omega^2 - D(z)|\vec{q}|^2}}, \tag{18}$$

where $F(z) = \dfrac{z^4}{z_h^4(1 - a^2)}$. For $a = 0$, this equation reduces to the SYM expression [19, 20]. Equation (18) shows that the particle carries spatial momentum in the x_1 or x_2 direction.

In the parallel case, the particle carries spatial momentum in the x_3 direction. The corresponding stopping distance is

$$x_\parallel = \int_0^{z_h} dz \frac{\left(-aF(z)\omega + (1 - F(z))|\vec{q}|\right)}{D(z)\sqrt{\left[(1 + a^2 F(z))\omega^2 + 2aF(z)\omega|\vec{q}| - (1 - F(z))|\vec{q}|^2\right]}}. \tag{19}$$

As discussed in [42], we consider a planar black brane at high temperature. Moreover, we restrict the rotation parameter to the stable regime $|a| < 0.75$. We investigate the dependence of the light-quark stopping distance on the rotation parameter in the spinning black-hole back-

CPC Accepted

ground, which is dual to a rigidly rotating fluid. In the numerical calculations, to keep the dimensionless initial radial position fixed during the scan over a, we use the fixed lower and upper cutoffs $z_0 = \zeta_0 z_h$ and $z_{\rm end} = (1-\delta)z_h$, with $\zeta_0 = 8\times10^{-3}$ and $\delta = 10^{-4}$.

The left panel of Fig. 1 displays the stopping distance of a light quark as a function of temperature T for fixed rotation parameter a. The stopping distance of light quarks decreases monotonically with increasing temperature, implying that they stop more readily in a hotter environment. Meanwhile, the anisotropy induced by the rotation of the medium also weakens as the temperature rises.

The right panel of Fig. 1 displays the dependence on the rotation parameter a at fixed $T = 80/\pi$. The transverse result is symmetric under $a \to -a$, reaches its maximum at $a = 0$, and decreases as $|a|$ increases. By contrast, the parallel result is asymmetric because the parallel geodesic equation contains terms linear in a, originating from the off-diagonal metric component $g_{\tau x_3}$. For the ultrarelativistic probe with fixed z_0/z_h and $z_{\rm end}/z_h$, the analytical derivation in Appendix A gives $x_{\parallel} = \dfrac{A - aB}{\pi T}$, where A and B are independent of a. Thus, the parallel stopping distance depends linearly on a, in agreement with the numerical results. In our setup, the probe propagates along the $+x_3$ direction. The parameter a controls the local rotational flow. Positive a corresponds to local medium flow along the negative x_3 direction and hence to a counter-propagating jet–medium configuration, leading to a reduced stopping distance. Negative a corresponds to a co-propagating configuration and increases the parallel stopping distance. At $a = 0$, the two curves coincide, as expected in the static isotropic limit. Therefore, in the co-propagating configuration, a light quark moving parallel to the medium flow travels farther before thermalizing than one moving transversely, whereas the opposite behavior occurs in the counter-propagating configuration.

B. Shooting string

In this subsection, we study light-quark energy loss using the shooting-string approach in the spinning Myers-Perry black hole background. In this approach [22, 23], a classical string endpoint starts near the horizon and propagates toward the boundary, carrying finite energy and momentum that are gradually transferred to the rest of the string.

Following [22, 23], we apply the shooting-string method to the background metric (10). The resulting instantaneous energy loss of a light quark is given by

$$\frac{dE}{dx^i} = \frac{1}{2\pi\alpha'}\frac{g_{\tau\nu}\dot{X}^\nu}{\dot{x}^i}, \tag{20}$$

The dot denotes differentiation with respect to the parameter λ along the endpoint worldline, $\dot{X}^\mu \equiv dX^\mu/d\lambda$, where $X^\mu = (\tau, x_1, x_2, x_3, z)$. We also define the conserved ratio $L = \frac{E}{q_{x_i}}$ to characterize the null geodesic. In the subsequent numerical calculations, we set $1/(2\pi\alpha') = 1$ for simplicity. A small value of z (i.e., an endpoint near the boundary) implies substantial energy loss, which would rapidly quench the jet and render it unobservable. Therefore, we require the strings to start close to the horizon.

We consider two propagation channels defined by the conserved spatial momentum of the string endpoint. In the transverse channel, the nonzero momentum is directed along x_1, whereas the conserved momentum along the rotational-flow direction vanishes, $q_3 = 0$. In the parallel channel considered separately below, the endpoint carries nonzero momentum along x_3. For the transverse channel, the conserved energy and momenta of the endpoint are

$$E_\perp = -\frac{1}{\eta}\left(g_{\tau\tau}\dot{\tau} + g_{\tau x_3}\dot{x}_3\right), \tag{21}$$

and

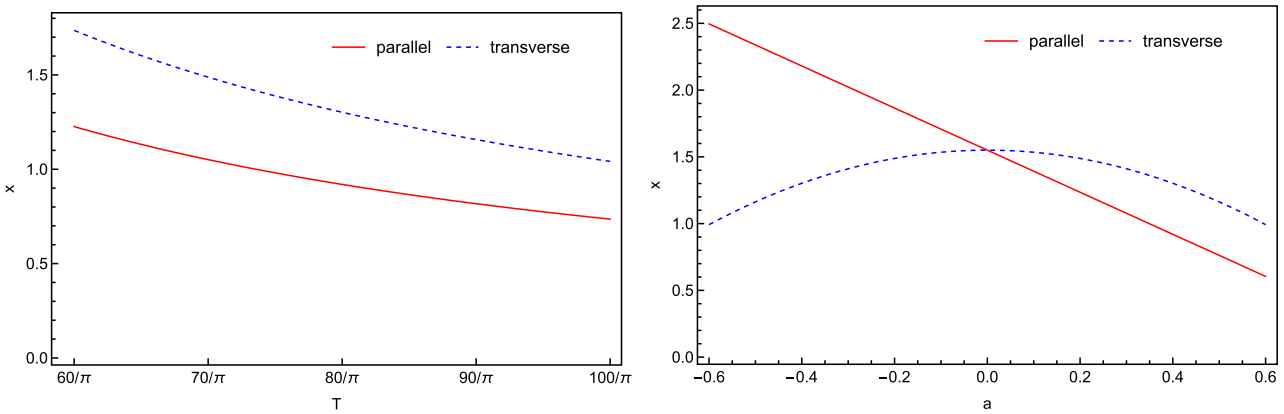

Fig. 1. (color online) **Left panel:** Stopping distance x as a function of the temperature T for $a = 0.4$. **Right panel:** Stopping distance x as a function of the rotation parameter a for $T = 80/\pi$.

CPC Accepted

$$q_{x_1} = \frac{1}{\eta} g_{x_1 x_1} \dot{x}_1, \qquad q_3 = \frac{1}{\eta}\left(g_{\tau x_3}\dot{\tau} + g_{x_3 x_3}\dot{x}_3\right) = 0, \tag{22}$$

where η is an auxiliary field. The metric components are $g_{\tau\tau} = -\dfrac{1-F(z)}{z^2}$, $g_{\tau x_3} = \dfrac{aF(z)}{z^2}$, $g_{x_3 x_3} = \dfrac{1+a^2F(z)}{z^2}$, and $g_{x_1 x_1} = \dfrac{1}{z^2}$. Therefore, the null geodesic equations become

$$L_\perp = \frac{E_\perp}{p_{x_1}} = \frac{f(z)\dot{\tau} - aF(z)\dot{x}_3}{\dot{x}_1}, \tag{23}$$

where $f(z) = 1 - \dfrac{z^4}{z_h^4(1-a^2)}$.

Imposing the null condition $ds^2 = 0$ and setting $q_3 = 0$, we obtain the transverse trajectory along x_1 and the associated induced drift along x_3:

$$\left(\frac{dx_1}{dz}\right)^2_\perp = \frac{1}{(1+a^2F(z))L_\perp^2 - D(z)}, \quad \left(\frac{dx_3}{dz}\right)^2_{\text{ind}} = \frac{a^2F(z)^2L_\perp^2}{D^2[(1+a^2F(z))L_\perp^2 - D(z)]}. \tag{24}$$

Because the metric contains the off-diagonal component $g_{\tau x_3}$, the condition $p_3 = 0$ does not imply $\dot{x}_3 = 0$. Instead, Eq. (21) gives $\dot{x}_3 = -\dfrac{g_{\tau x_3}}{g_{x_3 x_3}}\dot{\tau} = -\dfrac{aF(z)}{1+a^2F(z)}\dot{\tau}$. Thus, an endpoint with purely transverse conserved spatial momentum may acquire an induced coordinate drift along the x_3 direction. This drift originates from the off-diagonal metric component and should not be confused with the independent parallel-propagation channel considered below.

At the radial turning point $z = z_*$, the common radial denominator in (24) vanishes, yielding

$$L(z_*)_\perp = \sqrt{\frac{D(z_*)}{1+a^2F(z_*)}}. \tag{25}$$

Thus, the null trajectory in transverse-momentum configuration space becomes

$$\left(\frac{dx_1}{dz}\right)_\perp = -\sqrt{\frac{1+a^2F(z_*)}{F(z)-F(z_*)}}, \quad \left(\frac{dx_3}{dz}\right)_{\text{ind}} = \frac{aF(z)}{D(z)}\sqrt{\frac{D(z_*)}{F(z)-F(z_*)}}. \tag{26}$$

Only the first relation is required to evaluate the transverse energy-loss rate. The second relation describes the longitudinal coordinate drift induced by the rotational background.

Combining (10), (20), and (25) yields the light-quark energy loss

$$\left(\frac{dE}{dx_1}\right)_\perp = -\frac{L(z_*)_\perp}{2\pi\alpha' z^2}, \tag{27}$$

We now turn to the independent channel for parallel propagation. In this case, the endpoint carries nonzero conserved momentum along x_3, whereas the transverse momenta vanish, $q_1 = q_2 = 0$. The null geodesics can be obtained

$$L(z_*)_\parallel = \frac{-aF(z_*) + \sqrt{D(z_*)}}{1+a^2F(z_*)}, \tag{28}$$

where $F(z_*) = \dfrac{z_*^4}{z_h^4(1-a^2)}$ and $D(z_*) = 1 - \dfrac{z_*^4}{z_h^4}$.

The null geodesic equation for the parallel case is

$$\left(\frac{dx_3}{dz}\right)_\parallel = -\frac{1 - F(z) - aF(z)L(z_*)_\parallel}{D(z)\left(1+aL(z_*)_\parallel\right)\sqrt{F(z)-F(z_*)}}. \tag{29}$$

The light-quark energy loss in the parallel case is

$$\left(\frac{dE}{dx_3}\right)_\parallel = -\frac{1}{2\pi\alpha' z^2}\frac{L(z_*)_\parallel D(z)}{1-F(z)-aF(z)L(z_*)_\parallel}, \tag{30}$$

To better understand light-quark energy loss, we numerically integrate Eqs. (26) and (29) in the small-z_* limit and invert the results to obtain $z(x)$. We then substitute this expression into Eqs. (27) and (30), respectively. In asymptotically AdS_5 geometries, the shooting string approach typically takes $z_* \to 0$ [22, 23].

Fig. 2 summarizes the instantaneous energy loss of the shooting-string endpoint for parallel and transverse propagation. The boundary coordinate is denoted by x, with $x = x_3$ for parallel propagation and $x = x_1$ for transverse propagation. In the left panel, $a = 0.4$ and $x = 0.01$ are held fixed; the qualitative results are insensitive to the value of x. The energy-loss rates for both propagation directions increase monotonically with temperature, indicating that the endpoint loses energy more rapidly in a higher-temperature medium.

The middle panel shows the dependence on the rotation parameter a at fixed $T = 80/\pi$ and $x = 0.01$. The transverse result is symmetric under $a \to -a$, has its minimum at $a = 0$, and increases with $|a|$. This symmetry follows from the fact that transverse propagation depends on a only through even combinations. In contrast, the parallel energy loss is strongly asymmetric and increases monotonically with a, owing to the terms linear in a generated by the off-diagonal metric component $g_{\tau x_3}$. According to the convention $q_3 > 0$ adopted for the shooting-string endpoint, a counter-propagating jet-medium configuration ($a > 0$) enhances energy loss, whereas a co-propagating configuration ($a < 0$) suppresses the parallel energy loss. The parallel rate grows more rapidly than the

CPC Accepted

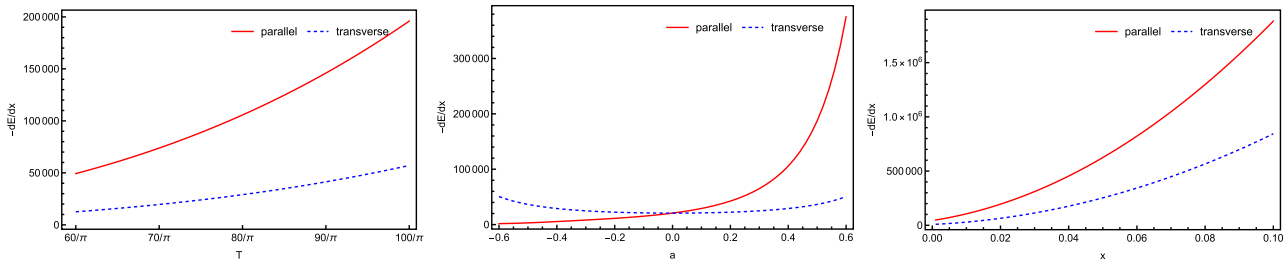

Fig. 2. (color online) **Left panel:** Instantaneous energy loss $-dE/dx$ as a function of temperature T with $a = 0.4$ and $x = 0.01$. **Middle panel:** Instantaneous energy loss $-dE/dx$ as a function of the rotation parameter a with $T = 80/\pi$ and $x = 0.01$. **Right panel:** Instantaneous energy loss $-dE/dx$ as a function of the boundary spatial coordinate x, evaluated along the endpoint trajectory, with $T = 80/\pi$ and $a = 0.4$.

transverse rate because the parallel expression contains an additional a-dependent factor. Consequently, in the negative-a region shown in the figure, the transverse energy-loss rate is larger than the parallel one, $(-dE/dx_1)_\perp > (-dE/dx_3)_\parallel$. For positive a, this ordering is reversed: the counter-propagating kinematics enhance the parallel energy-loss rate, leading to $(-dE/dx_3)_\parallel > (-dE/dx_1)_\perp$, with the difference between the two orientations becoming increasingly pronounced as a increases.

The right panel presents the position dependence of the energy-loss rate at fixed $T = 80/\pi$ and $a = 0.4$. Here, x is the running boundary spatial coordinate evaluated along the shooting-string endpoint trajectory and should not be confused with the stopping distance, despite the shared notation. As the endpoint propagates outward from the near-horizon region toward the boundary, its radial coordinate $z(x)$ decreases. Consequently, the factor $1/z^2(x)$ appearing in the energy-loss formulas produces a nonlinear increase in $-dE/dx$ with x.

These results are qualitatively consistent with those in Fig. 1 and show that both the local radial position of the string endpoint and the relative motion between the probe and the medium play essential roles in determining the instantaneous energy-loss rate.

IV. CONCLUSION AND DISCUSSION

In this work, we investigate light-quark energy loss in a rotating, strongly coupled plasma using holography. We employ both the falling-string and shooting-string descriptions. The gravitational background is obtained from the large-black-hole limit of the spinning Myers-Perry geometry and can be interpreted as a boosted/spinning black brane. In this setup, the parameter a controls the strength of the boost/rotational effects of the dual fluid.

Our results reveal a consistent physical picture across the two string descriptions. Increasing the temperature enhances light-quark quenching: the falling-string analysis yields a shorter propagation distance before thermalization, whereas the shooting-string analysis gives a larger instantaneous energy-loss rate. For transverse motion, increasing the magnitude of the rotation parameter enhances energy loss. For parallel motion, however, the relative direction between the quark and the medium flow is crucial: a counter-propagating configuration enhances energy loss and leads to earlier stopping, whereas a co-propagating configuration suppresses energy loss and allows the quark to propagate farther. In the static limit, the parallel and transverse results coincide, as required by isotropy. Moreover, the shooting-string energy loss increases nonlinearly as the endpoint moves from the near-horizon region toward the boundary. Thus, both approaches consistently show that stronger instantaneous energy loss corresponds to a shorter distance before thermalization.

From the boundary-fluid viewpoint, the observed directional dependence arises from the relative motion between the energetic quark and the local rotational flow. The present planar approximation captures only this local kinematic effect of rotation, whereas effects associated with finite-size geometry, velocity gradients, vorticity, and centrifugal acceleration [49] require an analysis beyond the strict planar limit. Finally, the classical string description used here does not resolve the intrinsic spin of the light-quark excitation and does not include spin–rotation or spin–vorticity couplings. The results should therefore be understood as classical stopping and energy-dissipation results in the local planar limit. Our results are in qualitative agreement with previous holographic studies of rotational effects on heavy-quark dynamics [36, 37] and on the jet-quenching parameter in rotating plasmas [38, 47].

Several extensions are worth pursuing. In particular, it would be interesting to study light-quark energy loss in a rotating background with finite chemical potential, such as a charged rotating black hole background [50]. This would make it possible to explore the combined effects of rotation and density on parton energy loss, which may be relevant for a more realistic description of strongly coupled QCD matter.

ACKNOWLEDGMENTS

Yan-Qing Zhao is supported by the National Natural

CPC Accepted

Science Foundation of China (NSFC) under Grant No. 12505151. Zhou-Run Zhu is supported by the Natural Science Foundation of Henan Province, China, under Grant No. 242300420947, and by the Startup Foundation for Doctors at Zhoukou Normal University under Project No. ZKNUC2023018.

Appendix A: Analytical derivation of stopping distance in parallel case

For a probe propagating in the positive x_3 direction, we make the ultrarelativistic choice $q_3 = \omega > 0$. The radicand in the equation for the parallel trajectory, Eq. (19), then simplifies to

$$\mathcal{R}_{\parallel} = (1+a^2F)\omega^2 + 2aF\omega q_3 - (1-F)q_3^2 = \omega^2(1+a)^2F. \quad \text{(A1)}$$

The corresponding numerator becomes

$$-aF\omega + (1-F)q_3 = \omega\left[1-(1+a)F\right]. \quad \text{(A2)}$$

Thus, for $|a|<1$, the cutoff-regulated parallel stopping distance is

$$x_{\parallel} = \int_{z_0}^{(1-\delta)z_h} \frac{1-(1+a)F}{D(1+a)\sqrt{F}}\,dz. \quad \text{(A3)}$$

Introducing $u = z/z_h$ and using $z_h = \sqrt{1-a^2}/(\pi T)$, we obtain

$$\begin{aligned} x_{\parallel}(T,a) &= \frac{1}{\pi T}\int_{\zeta_0}^{1-\delta} \frac{1-a-u^4}{u^2(1-u^4)}\,du \\ &= \frac{1}{\pi T}\left[\int_{\zeta_0}^{1-\delta}\frac{du}{u^2} - a\int_{\zeta_0}^{1-\delta}\frac{du}{u^2(1-u^4)}\right]. \end{aligned} \quad \text{(A4)}$$

Therefore,

$$x_{\parallel}(T,a) = \frac{A-aB}{\pi T} \quad \text{(A5)}$$

with

$$\begin{aligned} A &= \frac{1}{\zeta_0} - \frac{1}{1-\delta}, \\ B &= \int_{\zeta_0}^{1-\delta}\frac{du}{u^2(1-u^4)} = \left[-\frac{1}{u} + \frac{1}{2}\left(\operatorname{artanh} u - \arctan u\right)\right]_{\zeta_0}^{1-\delta}. \end{aligned} \quad \text{(A6)}$$

Because the integration limits are fixed and lie within $(0,1)$, A and B are independent of a, with $B>0$. It follows that

$$\left.\frac{\partial x_{\parallel}}{\partial a}\right|_T = -\frac{B}{\pi T} < 0, \qquad \left.\frac{\partial^2 x_{\parallel}}{\partial a^2}\right|_T = 0. \quad \text{(A7)}$$

Thus, at fixed temperature, the parallel stopping distance is an exactly linear function of a under the stated assumptions.

The exact linear dependence established above applies to the present ultrarelativistic calculation with fixed ζ_0 and δ. It is not a general result for arbitrary $\omega/|q_3|$ or for other initial-position prescriptions.

CPC Accepted

References

[1] I. Arsene *et al.* [BRAHMS Collaboration], Nucl. Phys. A **757**, 1 (2005), arXiv: nucl-ex/0410020

[2] K. Adcox *et al.* [PHENIX Collaboration], Nucl. Phys. A **757**, 184 (2005), arXiv: nucl-ex/0410003

[3] B. B. Back *et al.*, Nucl. Phys. A **757**, 28 (2005), arXiv: nucl-ex/0410022

[4] J. Adams *et al.* [STAR Collaboration], Nucl. Phys. A **757**, 102 (2005), arXiv: nucl-ex/0501009

[5] X. N. Wang and M. Gyulassy, Phys. Rev. Lett. **68**, 1480 (1992)

[6] R. Baier, Y. L. Dokshitzer, A. H. Mueller, S. Peigne and D. Schiff, Nucl. Phys. B **483**, 291 (1997), arXiv: hep-ph/9607355[hep-ph]

[7] A. Majumder and M. Van Leeuwen, Prog. Part. Nucl. Phys. **66**, 41 (2011), arXiv: 1002.2206[hep-ph]

[8] G. Y. Qin and X. N. Wang, Int. J. Mod. Phys. E **24**(11), 1530014 (2015), arXiv: 1511.00790[hep-ph]

[9] E. V. Shuryak, Nucl. Phys. A **750**, 64 (2005), arXiv: hep-ph/0405066[hep-ph]

[10] P. Kovtun, D. T. Son and A. O. Starinets, Phys. Rev. Lett. **94**, 111601 (2005), arXiv: hep-th/0405231[hep-th]

[11] J. M. Maldacena, Adv. Theor. Math. Phys. **2**, 231 (1998), arXiv: hep-th/9711200[hep-th]

[12] E. Witten, Adv. Theor. Math. Phys. **2**, 253 (1998), arXiv: hep-th/9802150[hep-th]

[13] S. S. Gubser, I. R. Klebanov and A. M. Polyakov, Phys. Lett. B **428**, 105 (1998), arXiv: hep-th/9802109[hep-th]

[14] J. Casalderrey-Solana, H. Liu, D. Mateos, K. Rajagopal and U. Achim Wiedemann, Cambridge University Press, 2014, ISBN 978-1-009-40350-4, 978-1-009-40349-8, 978-1-009-40352-8, 978-1-139-13674-7 doi: 10.1017/9781009403504 [arXiv: 1101.0618 [hep-th]].

[15] O. DeWolfe, S. S. Gubser, C. Rosen and D. Teaney, Prog. Part. Nucl. Phys. **75**, 86 (2014), arXiv: 1304.7794[hep-th]

[16] H. Liu, K. Rajagopal and U. A. Wiedemann, Phys. Rev. Lett. **97**, 182301 (2006), arXiv: hep-ph/0605178[hep-ph]

[17] H. Liu, K. Rajagopal and U. A. Wiedemann, JHEP **03**, 066 (2007), arXiv: hep-ph/0612168[hep-ph]

[18] P. M. Chesler, K. Jensen, A. Karch and L. G. Yaffe, Phys. Rev. D **79**, 125015 (2009), arXiv: 0810.1985[hep-th]

[19] P. Arnold and D. Vaman, JHEP **10**, 099 (2010), arXiv: 1008.4023[hep-th]
[20] P. Arnold and D. Vaman, JHEP **04**, 027 (2011), arXiv: 1101.2689[hep-th]
[21] P. M. Chesler, K. Jensen and A. Karch, Phys. Rev. D **79**, 025021 (2009), arXiv: 0804.3110[hep-th]
[22] A. Ficnar and S. S. Gubser, Phys. Rev. D **89**(2), 026002 (2014), arXiv: 1306.6648[hep-th]
[23] A. Ficnar, S. S. Gubser and M. Gyulassy, Phys. Lett. B **738**, 464 (2014), arXiv: 1311.6160[hep-ph]
[24] Z. R. Zhu, S. Q. Feng, Y. F. Shi and Y. Zhong, Phys. Rev. D **99**(12), 126001 (2019), arXiv: 1901.09304[hep-ph]
[25] Z. q. Zhang, X. Zhu and D. f. Hou, Eur. Phys. J. C **83**(5), 389 (2023)
[26] Z. q. Zhang, Eur. Phys. J. C **79**(12), 992 (2019)
[27] Z. q. Zhang, Phys. Lett. B **793**, 308 (2019)
[28] L. Zhang, L. Yin, G. D. Zhou, C. J. Fan and X. Chen, Phys. Rev. D **111**(12), 126001 (2025), arXiv: 2504.04979[hep-ph]
[29] Z. T. Liang and X. N. Wang, Phys. Rev. Lett. **94**, 102301 (2005), arXiv: nucl-th/0410079[nucl-th]
[30] F. Becattini, F. Piccinini and J. Rizzo, Phys. Rev. C **77**, 024906 (2008), arXiv: 0711.1253[nucl-th]
[31] M. Baznat, K. Gudima, A. Sorin and O. Teryaev, Phys. Rev. C **88**(6), 061901 (2013), arXiv: 1301.7003[nucl-th]
[32] L. Adamczyk *et al*. [STAR], Nature **548**, 62 (2017), arXiv: 1701.06657[nucl-ex]
[33] Y. Jiang, Z. W. Lin and J. Liao, Phys. Rev. C **94**(4), 044910 (2016), arXiv: 1602.06580[hep-ph]
[34] X. Chen, L. Zhang, D. Li, D. Hou and M. Huang, JHEP **07**, 132 (2021), arXiv: 2010.14478[hep-ph]
[35] Y. Q. Zhao, S. He, D. Hou, L. Li and Z. Li, JHEP **04**, 115 (2023), arXiv: 2212.14662[hep-ph]
[36] A. A. Golubtsova, E. Gourgoulhon and M. K. Usova, Nucl. Phys. B **979**, 115786 (2022), arXiv: 2107.11672[hep-th]
[37] I. Y. Aref'eva, A. A. Golubtsova and E. Gourgoulhon, JHEP **04**, 169 (2021), arXiv: 2004.12984[hep-th]
[38] A. A. Golubtsova and N. S. Tsegelnik, Phys. Rev. D **107**(10), 106017 (2023), arXiv: 2211.11722[hep-th]
[39] S. W. Hawking, C. J. Hunter and M. Taylor, Phys. Rev. D **59**, 064005 (1999), arXiv: hep-th/9811056[hep-th]
[40] G. W. Gibbons, M. J. Perry and C. N. Pope, Class. Quant. Grav. **22**, 1503 (2005), arXiv: hep-th/0408217[hep-th]
[41] G. W. Gibbons, H. Lu, D. N. Page and C. N. Pope, Phys. Rev. Lett. **93**, 171102 (2004), arXiv: hep-th/0409155[hep-th]
[42] M. Garbiso and M. Kaminski, JHEP **12**, 112 (2020), arXiv: 2007.04345[hep-th]
[43] M. A. G. Amano, C. Cartwright, M. Kaminski and J. Wu, Prog. Part. Nucl. Phys. **139**, 104135 (2024), arXiv: 2308.11686[hep-th]
[44] Z. R. Zhu, S. Wang, X. Chen, J. X. Chen and D. Hou, Phys. Rev. D **110**(12), 126008 (2024), arXiv: 2407.03633[hep-ph]
[45] Z. R. Zhu, M. Sun, R. Zhou, Z. Ma and J. Han, Eur. Phys. J. C **84**(12), 1252 (2024), arXiv: 2406.19661[hep-ph]
[46] Z. R. Zhu, S. Wang, Y. K. Liu and D. Hou, Phys. Rev. D **112**(2), 026012 (2025), arXiv: 2501.04318[hep-ph]
[47] Z. R. Zhu, S. Wang, M. L. Tian and D. Hou, Phys. Rev. D **113**(6), 066014 (2026), arXiv: 2512.13076[hep-ph]
[48] K. Murata, Prog. Theor. Phys. **121**, 1099 (2009), arXiv: 0812.0718[hep-th]
[49] J. X. Chen, D. F. Hou and H. C. Ren, JHEP **03**, 171 (2024), arXiv: 2308.08126[hep-ph]
[50] M. Cvetic, H. Lu and C. N. Pope, Phys. Lett. B **598**, 273 (2004), arXiv: hep-th/0406196[hep-th]

CPC Accepted